Proceedings of the ASME 2023
Pressure Vessels & Piping Conference
PVP2023
July 16-21, 2023, Atlanta, Georgia, USA

PVP2023-102314

PIPELINE STACKED CRACK INTERACTION BURST PRESSURE ANALYSIS USING 3-D CRACK MESHES

Ryan Holloman[1], Greg Thorwald[1], Michael Turnquist[1], Mark Neuert[2]

[1]Quest Integrity USA, LLC, Boulder, Colorado, USA
[2]Enbridge, Edmonton, AB, Canada

ABSTRACT

Accurate evaluation of the remaining strength of crack-like flaws identified via pipeline inline inspection (ILI) or in-ditch non-destructive examination (NDE) is critical to ensuring continued safe operation of liquid and gas transmission pipelines. Modern pipeline ILI tools have sufficient resolution to detect longitudinally overlapping crack-like flaws that exist in the same radial plane, referred to as stacked cracks. Depending upon the crack sizes and pressure loading, stacked cracks can interact to reduce burst pressure below that of any of the individual stacked cracks.

Closely located cracks are often evaluated using interaction criteria, such as those provided by API 579-1/ASME FFS-1 Part 9 (API 579) [1], which specify how and when multiple nearby cracks can be combined into a single crack for the purpose of an integrity assessment. When applied to stacked cracks, the interaction criteria can often lead to recategorizing stacked cracks as a through-wall crack, which requires urgent response from the pipeline operator.

Here, an improved interaction criterion was developed for stacked cracks based on the results of elastic-plastic finite element analysis (FEA) models of multiple combinations of stacked crack sizes and orientations, pipe material properties, and operating stress. These improved interaction criteria provide pipeline operators with an easy-to-apply methodology to analyze stacked cracks that reduces the excess conservatism associated with legacy methods.

Keywords: Pipeline Integrity, Stacked Cracks, Crack Interaction Criteria, Elastic-Plastic FEA, Fracture Mechanics, Crack Mesh.

NOMENCLATURE

a_{ext}	Crack Depth for External Crack
a_{int}	Crack Depth for Internal Crack
α	Ramberg-Osgood Fitting Parameter
COV	Coefficient of Variation
ID	Inner Diameter
Kc	Toughness
l	Remaining ligament
MOP	Maximum Operating Pressure
n	Ramberg-Osgood Hardening Exponent
NWT	Nominal Wall Thickness
OD	Outer Diameter
PC	Plastic Collapse
s	Single Crack
st	Stacked Crack
SMYS	Specified Minimum Yield Strength
WT	Wall Thickness

1. INTRODUCTION

Assessment of crack-like anomalies in pipelines is necessary to a comprehensive pipeline integrity program. Crack assessment models enable pipeline operators to estimate burst pressures associated with cracks of a given dimension in a pipe of given properties and geometry; however, these models typically assume a singular crack in isolation, i.e., not interacting with other nearby cracks.

Some guidance exists on how to assess whether nearby cracks are expected to interact, as well as how to approach the assessment of such a multi-crack system. The widely adopted CorLAS crack burst pressure model [2] can be used to iteratively evaluate different combinations of profiles from cracks in close proximity to yield either an equivalent crack or the conclusion that evaluating the involved cracks in isolation is the most conservative approach. Industry-recommended practices such as API 579 [2] provide guidance on combining cracks that are in the same circumferential plane into a single equivalent geometry based on axial and radial separation distances (Figure 1). In these cases, it is assumed that assessing the single equivalent crack results in a conservative burst pressure compared to the multi-crack system.

Multiple Crack-Like Flaw Configuration	Criterion For Interaction	Effective Dimensions After Interaction
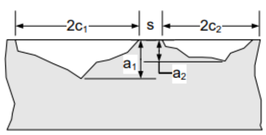 Configuration 1	$s\ \delta\ \max\rangle 0.5a_1,\ 0.5a_2$≚	$2c\quad 2c_1 + 2c_2 + s$ $a\quad \max\rangle a_1,\ a_2$≚
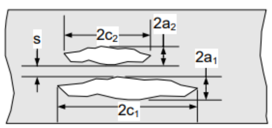 Configuration 2	$s\ \delta\ \max\rangle a_1,\ a_2$≚	$2a\quad 2a_1 + 2a_2 + s$ $2c\quad \max\rangle 2c_1,\ 2c_2$≚
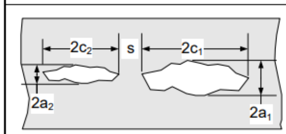 Configuration 3	$s\ \delta\ \max\rangle a_1,\ a_2$≚	$2c\quad 2c_1 + 2c_2 + s$ $2a\quad \max\rangle 2a_1,\ 2a_2$≚
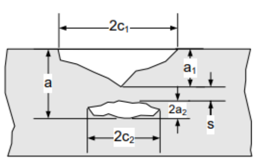 Configuration 4	$s\ \delta\ \max\rangle 0.5a_1,\ a_2$≚	$a\quad a_1 + 2a_2 + s$ $2c\quad \max\rangle 2c_1,\ 2c_2$≚

FIGURE 1: EXAMPLE FROM API 579 FOR COMBINING CRACKS [1]

However, both approaches have limitations. Using CorLAS to combine cracks is only applicable to same-sided surface-breaking cracks; i.e., both cracks must be on the inner diameter (ID) or outer diameter (OD) of the pipe, and API 579 provides no insight regarding the degree of conservatism inherent in the recommended equivalent crack configurations. In fact, these interaction criteria can lead to recategorizing cracks as a through-wall crack that requires urgent response from the pipeline operator, which may be an overly conservative approach and lead to unnecessary mitigative actions. Furthermore, like CorLAS, API 579 provides no explicit guidance on how to approach two surface-breaking cracks on the ID and OD of the pipe that overlap axially (hereafter referred to as “stacked” cracks).

With the advent of high-resolution ultrasonic crack detection tools used in ILI and NDE, stacked crack-like defects such as lack-of-fusion (LOF) and hook cracks are being reported with increased frequency in the longitudinal seam of pipes manufactured using low-frequency electric resistance welding (LF-ERW) and flash welding (FW). Considering that these crack-like defects are known to be responsible for a large proportion of past in-service and hydrostatic test failures [3], the ability to understand conditions under which stacked cracks would be expected to interact, and to model the stacked crack system as a single equivalent crack with an associated level of conservatism, is of great use to pipeline operators. Thus, Enbridge partnered with Quest Integrity to develop three-dimensional (3-D) finite element (FE) models of pipes with stacked cracks to explore the behavior of stacked and non-stacked cracks for different combinations of crack depth, pipe geometry, and pipe material properties.

3-D FEA using appropriate crack meshing techniques [4] is an alternative to the API 579 Part 9 criteria. Detailed FEA allows estimation of pipeline burst pressure based on customized combinations of crack geometry, pressure loading, and material properties, which may reduce the conservatism inherent in the Part 9 criteria and allow for analysis of cases not explicitly covered in the guidance. In particular, the case of stacked internal and external surface-breaking cracks, a scenario commonly reported by ILI tools, are not explicitly covered under the Part 9 criteria.

Elastic-plastic FEA of cracks uses concentric rings of brick elements along the crack front to compute the crack front J-integral values over several contours as a function of increasing internal pressure. The crack front brick elements are initially collapsed on one element face with a set of initially coincident nodes that can displace as loading increases. This behavior helps capture crack front blunting as plasticity develops along the crack front with increasing pressure. The crack meshes use 20-node reduced integration elements. A crack driving force assessment of the stacked cracks then combines the J-integral results with the method in API 579 Part 9 Annex 9G.5 to determine burst pressure for a given pipeline steel toughness, Kc.

Depending on the size of the stacked cracks and the pressure loading level, a high-stress region in the ligament between the stacked cracks can develop. As the plastic zone in the ligament increases, so also the interaction of the stacked cracks. For closely spaced stacked cracks, the results show crack interaction begins at low pressure. For widely spaced stacked cracks, the results show crack interaction can still occur at higher pressure loads.

1.1 Pipe Selection

This section details how the pipe dimensions were selected for simulations in this study.

1.1.1 Equal Stacked Cracks

The pipe geometries and material properties represent pipes on the Enbridge system, where stacked cracks are regularly reported by NDE and ILI. This includes the following configurations:

- NPS 16 grade X52 pipe with 0.25-inch NWT
- NPS 24 grade X52 pipe with 0.281-inch NWT

- NPS 12 grade X52 pipe with 0.219-inch NWT
- NPS 16 grade X46 pipe with 0.315-inch NWT

It was hypothesized that WT would have a greater influence on crack interaction than pipe diameter given an assumed MOP of 72% SMYS. Therefore, the following geometry configurations were added to identify any trends with respect to wall thickness could be observed:

- NPS 16 grade X52 pipe with 0.219-inch NWT
- NPS 16 grade X52 pipe with 0.281-inch NWT
- NPS 16 grade X52 pipe with 0.315-inch NWT

Modified interaction criteria were adapted from configuration 4 in Figure 1 to predict when stacked surface-breaking cracks might interact. Given a set of stacked cracks of depth a_{ext} and a_{int} with a remaining ligament of

$$l = w.t. - a_{ext} - a_{int} \quad (1)$$

interaction is predicted to occur when

$$l \leq max(0.5\ a_{ext}, 0.5\ a_{int,}) \quad (2)$$

Assuming equal cracks, the minimum depth required for interaction is 0.4 x WT. Therefore, crack depth levels for the case of equal depths were set to 32.5% and 40% of WT to achieve scenarios below and at depths where interaction would be predicted to occur based on the above equation. Also, given the crack depths and pipe geometries described above, a single crack length of 2 inches (50.8 mm) was chosen for all stacked cracks.

1.1.2 Unequal Stacked Cracks

For the unequal stacked cracks, only the four pipe geometries that represent pipes on the Enbridge system, discussed in Section 1.1.1, were simulated.

Because crack depths below 40% through-wall were not predicted to interact based on equation 2, 40% through-wall was used as the lower bound of the deeper of the stacked crack pairs, with 60% through-wall being an upper bound because that size of crack would be mitigated by a pipeline operator if detected. For the shallower crack of the unequal stacked crack pair, a depth was selected such that the combined depth of both cracks ranged from 70% through-wall up to a depth that interaction was predicted by equation 2. To maintain consistency with the equal depth cases, a crack length of 2 inches (50.8 mm) was maintained here.

2. NUMERICAL CRACK MODELS

FE techniques have been used to investigate the interaction between stacked surface-breaking cracks compared to single surface-breaking cracks located axially along a pipelines axial plane.

2.1 Finite Element Models

The image in Figure 2(a) shows a quarter symmetric cylinder pipe mesh for a 12.75-inch (32.385-cm) OD pipe with a stacked crack located in the upper right portion of the image. A symmetry plane cuts through the pipe’s cross-section in the middle of the surface-breaking cracks at the right end of the mesh. Another symmetry plane cuts through the cylinder in the axial direction, resulting in a quarter symmetric model. The pipe’s symmetry was leveraged to reduce numerical run times.

Figure 2(b) is a close-up of stacked cracks that both measure 2 inches (50.8 mm) in the axial direction—one is an external axial surface-breaking crack and the other is an internal axial surface-breaking crack. The internal and external surface-breaking cracks are the halved, semi-elliptical regions. The highly refined focused crack mesh regions with concentric rings of elements around the crack front are used to compute the crack front J-integral and equivalent stress intensity values along the crack front in the FEA solver [5]. The brick elements in the first contour at the crack front have a collapsed element face with a set of initially coincident nodes at the crack front. The mid-side nodes of the first contour brick elements remain at the element mid-side location for the elastic-plastic analysis. The initially coincident crack front nodes can displace to capture crack front blunting as the applied pressure load increases and yielding occurs near the crack front. In the post-processing, the J-integral results are averaged using contours two through six (first contour omitted) to get the J-integral at each crack front node. Equivalent stress intensity, K, is computed from the J-integral values and material property values. API 579 Section 9G.3.5 details an approach for a focused mesh using elastic-plastic analysis, and Equation 9G.1 gives the K from J equation. Figure 2(c) shows a close-up at the crack depth location at the right end of the symmetry plane, where the highly refined mesh around the concentric ring elements is more apparent.

Figure 2(b) also shows the full length of the semi-elliptical stacked cracks. FEACrack™ [5] was used to build refined crack meshes. The cylinders were first partitioned to allow the external and internal crack depths to fit within two zones. In the case shown in Figure 2(b), the partition occurred at the mid-WT because the cracks are equal in depth in this example. Although for cases with unequal crack depths, the partition was located to allow the specified crack depths. Once the external and internal crack meshes were generated in each region, the two mesh regions were combined in a single input file for Abaqus [6] analysis. The two partitioned mesh regions were connected using the tied contact command in FEACrack™ to add the tied contact syntax in the Abaqus input file. Single cracks, which were either surface breaking on the external or internal side, were also modeled for comparison with the stacked crack stress intensity. The single crack models did not require partitioning; however, the crack meshes were identical for a direct comparison to the stacked cracks.

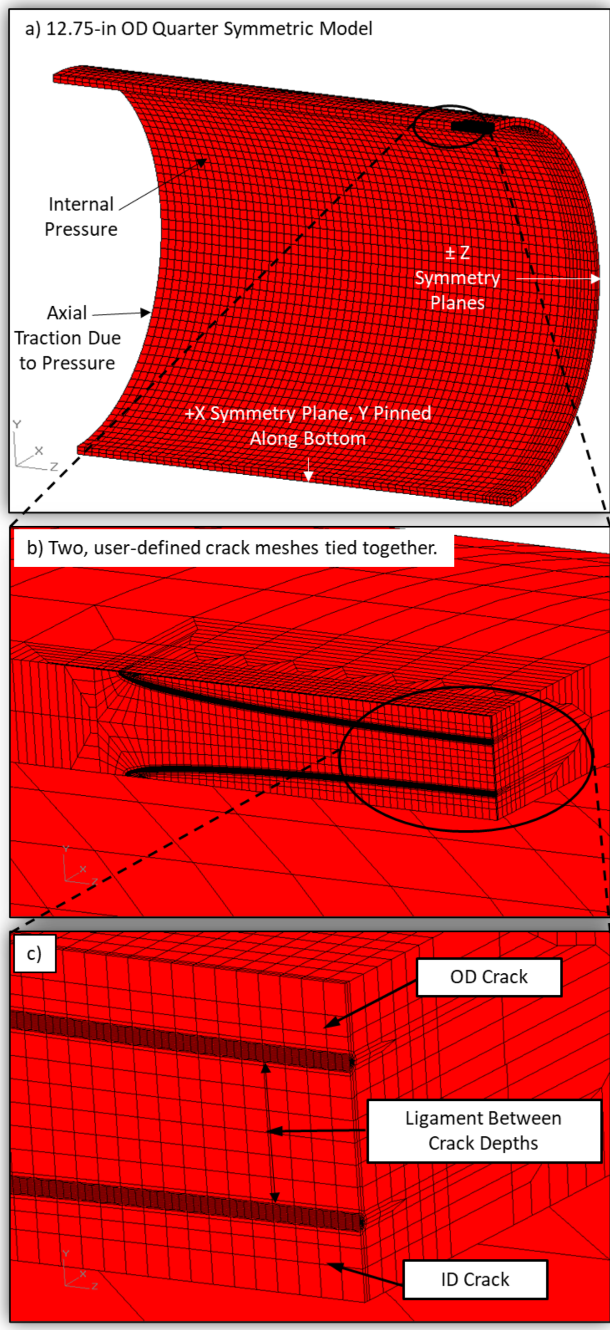

FIGURE 2: a) QUARTER SYMMETRIC STACKED CRACK MODEL WITH SYMMETRY CONSTRAINTS HIGHLIGHTED. b) A CLOSER VIEW OF THE STACKED CRACKS ALONG WITH A c) DETAILED VIEW OF REFINED CRACK FRONT ELEMENT.

Figure 2(a) highlights the symmetry constraints, internal pressure, and equivalent axial traction stress. The crack face pressure was applied to the internal surface crack partition.

Two vintage pipeline materials were explored here—one was X52 grade steel and the other was X46 grade steel. Table 1 summarizes the material properties assumed for the two steel grades explored. A feature in FEACrack™ automatically calculated Ramberg-Osgood curve-fit parameters, as shown in Table 1, which were used to obtain a table of stress-strain values for the Abaqus input file.

The pipe geometries and crack depths explored here are outlined in Tables 2 and 3. Table 2 represents stacked cracks that have equal external (a_{ext}) and internal (a_{int}) depths. The lengths remained constant at 2c = 2 inches (50.8 mm). Table 3 summarizes the scenarios that were explored with differing external (a_{ext}) and internal (a_{int}) depths. The unequal cracks also maintained a constant length of 2c = 2 inches (50.8 mm) for consistency. In addition, all the stacked crack scenarios shown in Tables 2 and 3 have corresponding single crack models to compare the stress intensity between the stacked cracks and identical single cracks.

TABLE 1: MATERIAL PROPERTIES APPLIED TO CRACK MODELS

Steel Grade	Modulus	Poisson's Ratio	Yield Strength	Tensile Strength	Ramberg-Osgood Parameters	
	Ksi (MPa)		Ksi (MPa)	Ksi (MPa)	n	α
X52	30,000 (206,842)	0.3	52 (358.5)	66 (455.1)	11.6	1.2
X46	30,000 (206,842)	0.3	46 (317.2)	63 (434.4	9.4	1.3

3. RESULTS AND DISCUSSION

This study first explored stacked cracks where a_{ext} and a_{int} are equal (Section 3.1). Next, unequal cracks were explored, where a_{int} was greater than a_{ext} (Section 3.2). Because the crack face pressure was applied to the internal surface crack, a_{int} was the deeper of the two cracks and the more conservative scenario.

3.1 Equal a_{ext} and a_{int} Crack Depths

The scenarios in Table 2 were explored for equal sized stacked cracks. In addition to the stacked cracks shown in Table 2, singular internal crack models were simulated for a direct comparison to identify when stacked cracks begin to interact. API 579 Part 9 provides an interaction rule for two surface breaking cracks, but the current guidance is conservative in that it does not specify the loading required for interaction to occur. Thus, this study sought to provide more specific interaction guidance to reduce repair costs.

Seven pipe geometries were explored, as outlined in Table 2. Each geometry simulated two equal crack scenarios; one where the crack depths were 32.5% of the WT and the other with 40% deep cracks. Based on the current API 579 interaction recommendations, none of the simulated cracks meets the interaction criteria. However, the simulations consistently showed that no interaction was observed when a_{ext} and a_{int} both equaled 32.5% of the WT. However, when crack depths were both increased to 40% of the WT, it was observed that the cracks begin to interact once the internal pressure reached 45% of SMYS.

TABLE 2: CRACK MODELS DEMONSTRATE THE PERCENTAGE OF SMYS WHERE CRACK INTERACTION STARTS WHEN THE OD AND ID CRACK DEPTHS ARE EQUAL

Pipe OD	Pipe WT	Pipe Grade	a_{ext} and a_{int} Crack Depths	Simulated Stacked Crack Interaction Begins at?	Meet API Crack Interaction Criteria
Inch (mm)	Inch (mm)		%	% SMYS	
12.75 (324)	0.219 (5.56)	X52	32.5	No interaction	NO
			40	45	NO
16 (406)	0.219 (5.56)	X52	32.5	No interaction	NO
			40	45	NO
16 (406)	0.25 (6.35)	X52	32.5	No interaction	NO
			40	45	NO
16 (406)	0.281 (7.14)	X52	32.5	No interaction	NO
			40	45	NO
16 (406)	0.314 (8.0)	X52	32.5	No interaction	NO
			40	45	NO
16 (406)	0.314 (8.0)	X46	32.5	No interaction	NO
			40	35	NO
24 (609)	0.281 (7.14)	X52	32.5	No interaction	NO
			40	45	NO

Figure 3 is a plot of the stress intensity K_J (equivalent K from J-integral results) versus pressure for a pipe geometry in Table 2 that measured 16-inches (406 mm) OD and 0.281-inch (7.14 mm) WT and had cracks with depths 40% of the WT. Stacked cracks and single ID cracks followed the same stress intensity trend until the pressure reached 45% of SMYS. At 45% of SMYS, the stacked cracks' stress intensity become non-linear, while the stress intensity for the single ID crack remained relatively linear. Thus, when the internal pressure reaches 45% of SMYS or greater, the cracks begin to interact, which differs from the guidance in API 579.

In addition, a curve labeled as a combined stack crack is shown. The combined curve assumes a_{ext} and a_{int} are summed to equal 80% of the WT for this example. This is important following a pipeline inspection because it highlights a conservative burst pressure if stacked cracks are characterized as a large singular surface crack.

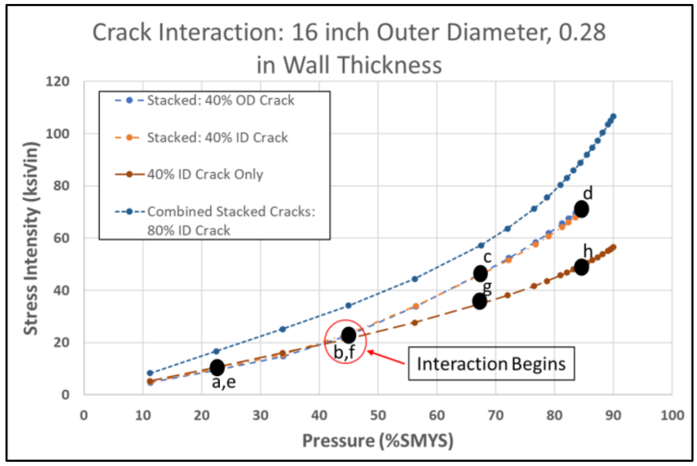

FIGURE 3: STRESS INTENSITY VERSUS PRESSURE FOR A 16-INCH (406-mm) OD AND 0.28-INCH (7.14-mm) WT PIPE WITH EQUAL STACKED CRACKS THAT MEASURE 40% OF THE WT.

The stress intensity versus pressure chart in Figure 3 highlights four unique pressure points with dark black circles. These increasing pressure points correspond to the montage of 3-D images shown in Figure 4, which highlight the effect of increasing stress along the crack front and in the ligament prior to yielding. Figure 4 shows the von Mises stress, where the maximum value is set to the yield strength of 52 ksi for this example (the maximum von Mises scale is always set to yield in the following figures). Figure 4(a) highlights an increase in the stacked cracks ligament stress, while a similar amount of stress is observed near the single ID cracks front in Figure 4(e), which corresponds to a similar stress intensity in Figure 3. Figure 4(b) and 4(f) are particularly interesting because these images correspond to the internal pressure where the stress intensity curves in Figure 3 begin to deviate at 45% SMYS. It is observed at 45% SMYS that the stress in the ligament increased in between the crack fronts, and the ligament is beginning to yield. The beginning of ligament yielding for the stacked crack allows the stress intensity curve in Figure 3 to become non-linear, while the single crack ligaments crack front is showing fewer signs of full yielding. Although the same relationship was observed for all the geometries with 40% deep cracks highlighted in Table 2, only one example is shown here.

Next, the case in which a_{ext} and a_{int} both equal 35% of the WT is explored for the same pipe geometry. The chart of stress intensity versus pressure is noticeably different in Figure 5 compared to Figure 4. Here, the stacked cracks behave similarly to the single surface-breaking ID crack, indicating minimal interaction between the stacked cracks. Again, four pressure points are explored, which are highlighted by four black dots in Figure 5. The shallower stacked cracks in Figure 6 compared to Figure 3 demonstrate that ligament yielding occurs at a higher pressure for shallower cracks. Figures 6(c) and 6(d) demonstrate the progression of yielding around the ligament, which is like Figure 4(b).

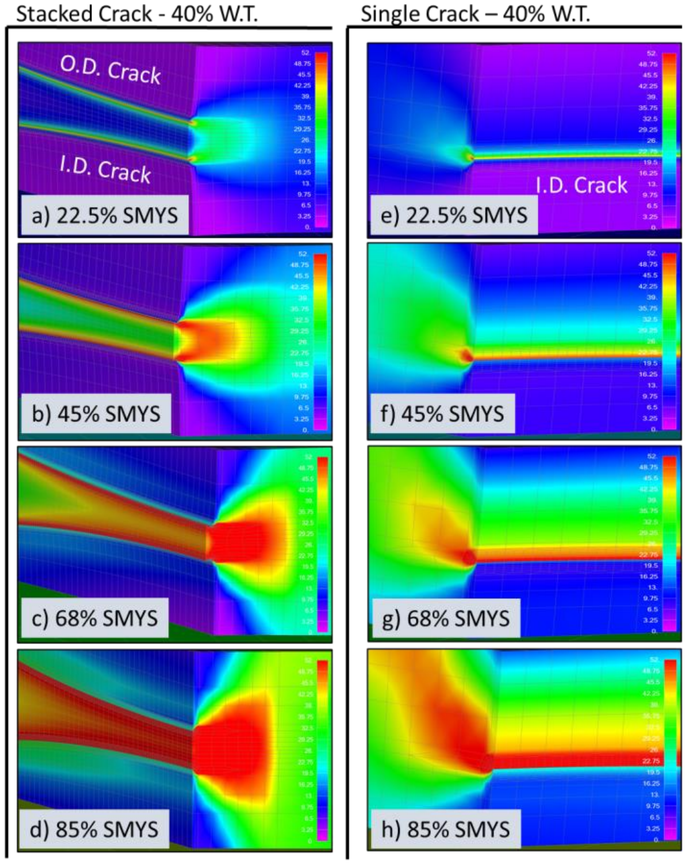

FIGURE 4: A MONTAGE OF THE VON MISES STRESS FOR EQUAL STACKED CRACKS THAT MEASURE 40% WT (a-d) AND A SINGLE ID CRACK THAT MEASURES 40% WT (e-h).

While the stress intensity curves for the stacked cracks are relatively like the single ID surface-breaking crack in Figure 5, a noticeable rise in stress intensity is observed for the stacked crack stress intensity curves. This rise is like the rise of Figure 3 at 45% SMYS. Thus, if the simulation was carried out past 72% SMYS in Figure 5 a non-linear response would likely be observed as the ligament completely approaches yield. Because it is unlikely a pipeline would be operated higher than 72% of SMYS, the simulation was not performed past 72% of SMYS. It is likely that crack interaction would occur at pressures greater than 72% SMYS because there is significant ligament yielding for the stacked crack in Figure 6(d), and the single crack ligament only experiences the start of yielding in Figure 6(h).

Figure 5 also plots the stress intensity for a combined stacked crack, which is the summation of a_{ext} and a_{int}. This demonstrates the level of conservatism if the stacked cracks are characterized as a singular ID surface-breaking crack. This level of conservatism could be the difference between a costly repair or continuing to monitor the defect location.

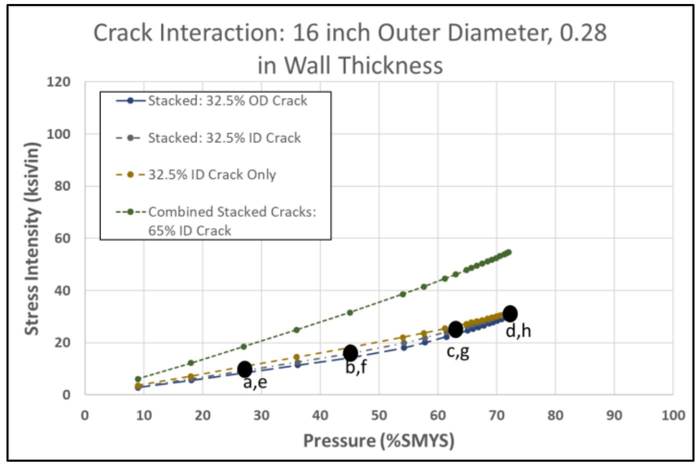

FIGURE 5: STRESS INTENSITY VERSUS PRESSURE FOR A 16-INCH (406-mm) OD AND 0.28-INCH (7.14-mm) WT PIPE WITH EQUAL STACKED CRACKS THAT MEASURE 32.5% OF THE WT.

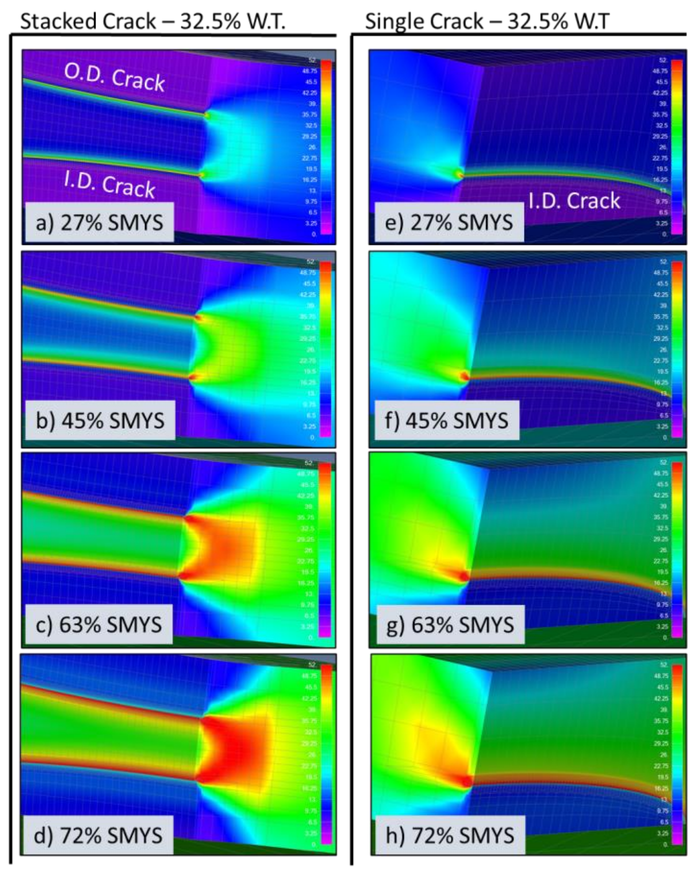

FIGURE 6: A MONTAGE OF THE VON MISES STRESS FOR EQUAL STACKED CRACKS THAT MEASURE 32.5% WT (a-d) AND A SINGLE ID CRACK THAT MEASURES 32.5% WT (e-h).

3.2 Unequal a_{ext} and a_{int} Crack Depths

After exploring equal stacked cracks in Section 3.1, this section investigates stacked cracks in which a_{ext} and a_{int} have different depths, which is like the unpredictable scenario observed after pipeline inspection is performed.

The results in Table 3 demonstrate a combination of depth scenarios that meet the current API 579 interaction criteria and others that do not meet the criteria. The simulations have shown that API 579 interaction criteria is not simply “Yes” or “No” because the crack sizes and pipe material dictate the pressure at which crack interaction is initiated. Because the internal crack has crack face pressure, it was decided to maintain it as the deeper of the two cracks for conservatism. The results in Table 3 suggest that when the ligament between the external and internal crack is greater than 27% of the WT, the cracks do not interact below 72% of SMYS, assuming the internal crack is 50% of the WT or less. When the internal crack exceeds 50% of the WT (as is the case of the 60% a_{int} crack in Table 3), interaction is possible at high stresses even when the ligament is greater than 27% of the WT due to increased rotation.

TABLE 3: CRACK MODELS DEMONSTRATE THE PERCENTAGE OF SMSYS WHERE CRACK INTERACTION STARTS WHEN THE OD AND ID CRACK DEPTHS ARE NOT EQUAL

Pipe OD	Pipe WT	Pipe Grade	a_{ext}/ a_{int} Crack Depths	Stacked Crack Interaction Begins at?	Meet API Crack Interaction Criteria
Inch (mm)	Inch (mm)		%	% SMYS	
16 (406)	0.25 (6.35)	X52	30/40	>70	NO
			35/40	55	NO
			40/40	45	YES
			20/50	No interaction	NO
			22.5/50	No interaction	NO
			25/50	>70	YES
			10/60	>60	YES
24 (609)	0.281 (7.14)	X52	30/40	>70	NO
			35/40	50	NO
			40/40	45	YES
			20/50	No interaction	NO
			22.5/50	No interaction	NO
			25/50	>70	YES
			10/60	>70	YES
12.75 (324)	0.219 (5.56)	X52	30/40	>70	NO
			35/40	45	NO
			40/40	45	YES
			20/50	No interaction	NO
			22.5/50	No interaction	NO
			25/50	>70	YES
			10/60	>60	YES
16 (406)	0.314 (8.0)	X46	30/40	>70	NO
			35/40	55	NO
			40/40	45	YES
			20/50	No interaction	NO
			22.5/50	No interaction	NO
			25/50	>70	YES
			10/60	>70	YES

The cracks with a_{int} = 50% of the WT showed no obvious crack interaction, as outlined in Table 3. A plot of the stress intensity versus pressure for a pipe with 16-inch (406-mm) OD, 0.25-inch WT, and 22.5% a_{ext} is shown in Figure 7. Unlike the equal stacked crack stress intensity profiles shown in Section 3.1, the OD and ID cracks have different stress intensity profiles due to different starting depths. Only the single ID surface crack was simulated for comparison because it is the deepest of the stacked cracks. The simulations were run to 72% of SMYS with no obvious deviation between the single and stacked ID crack in Figure 7. The four black pressure points in Figure 7 are explored with 3-D images in Figure 8. The von Mises stress profiles show very similar levels of yielding at the ligament for the stacked crack compared to the remaining ligament for the single crack. This observation suggests that the external stacked crack can be disregarded because it does not interact with the internal crack. This knowledge is also critical to understanding the way stacked cracks are re-categorized following pipeline inspection.

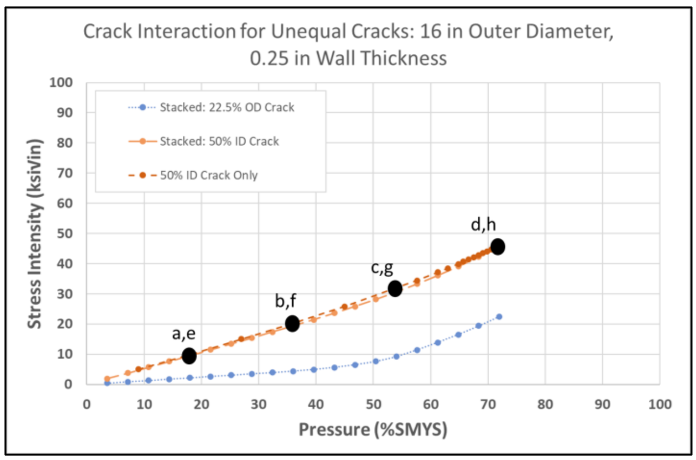

FIGURE 7: STRESS INTENSITY VERSUS PRESSURE FOR A 16-INCH (406-mm) OD AND 0.25-INCH (6.35-mm) WT PIPE WITH UNEQUAL STACKED CRACKS THAT MEASURE a_{ext} = 22.5% WT AND a_{int} = 50% of WT.

As a_{ext} is slightly increased from 22.5% to 25% of the WT, early signs of crack interaction are observed near 70% of SMYS, where the simulation stopped (Figure 9). However, prior to approximately 70% of SMYS, the results are nearly identical to those shown in Figure 7. API 579 interaction criteria state that the stacked cracks measuring a_{ext}/a_{int} = 25%/50% meet the interaction criteria. However, the simulations show that interaction does not occur unless the internal pressure is relatively high for typical pipeline operations.

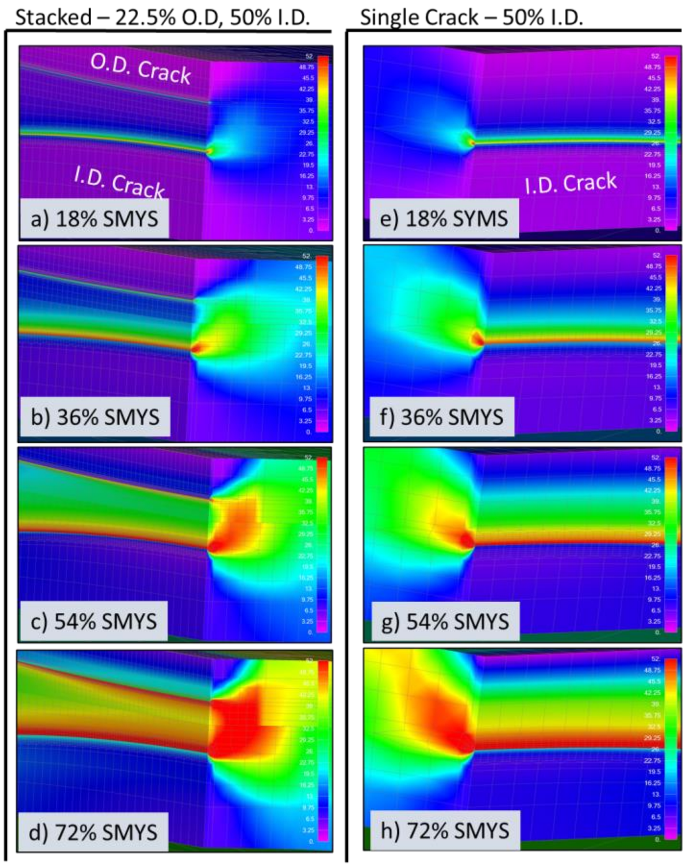

FIGURE 8: A MONTAGE OF THE VON MISES STRESS FOR UNEQUAL STACKED CRACKS THAT MEASURE a_{ext} = 22.5% WT AND a_{int} = 50% of WT. (a-d) AND A SINGLE ID CRACK THAT MEASURES 50% WT (e-h).

Next, stacked cracks with a_{int} = 40% of the WT are investigated. In Section 3.1, it was shown that when a_{ext}/a_{int} = 40%/40% crack interaction occurs at 45% SMYS. When the ligament is reduced to 30% of the WT, crack interaction is not observed until approximately 70% of SMYS (Figure 10). Reducing the stacked crack ligament to 25% of WT, which places it between a_{ext}/a_{int} = 40%/40% and a_{ext}/a_{int} = 30%/40% results in crack interaction occurring at approximately 55% of SMYS, as shown in Figure 11. Thus, the remaining ligament plays an important role in the amount of internal pressure required for crack interaction to initiate. The 3-D montage in Figure 12 that corresponds to the stress intensity curves in Figure 11 demonstrates that pressures below 45% SMYS have similar von Mises stresses (Figure 11[b] and 11[f]). However, Figures 11(c) and 11(g) demonstrate the plastic zone in the stacked crack has grown significantly more than the single crack plastic zone.

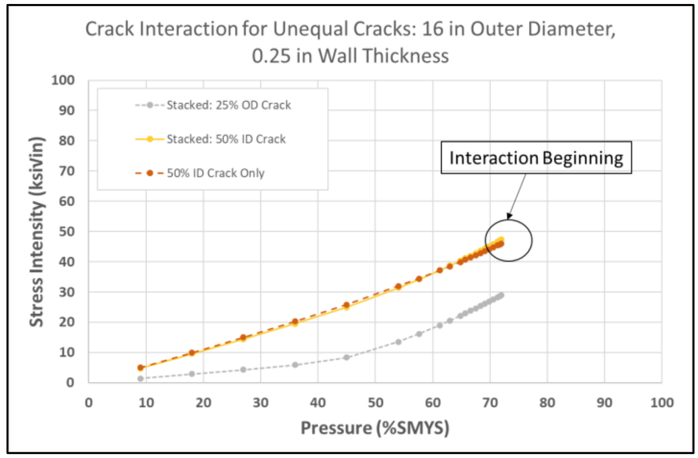

FIGURE 9: STRESS INTENSITY VERSUS PRESSURE FOR A 16-INCH (406-mm) OD AND 0.25-INCH (6.35-mm) WT PIPE WITH UNEQUAL STACKED CRACKS THAT MEASURE a_{ext} = 25% WT AND a_{int} = 50% WT.

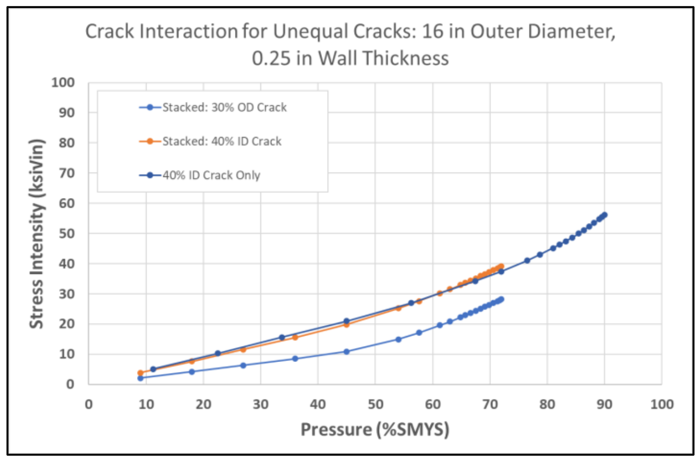

FIGURE 10: STRESS INTENSITY VERSUS PRESSURE FOR A 16-INCH (406-mm) OD AND 0.25-INCH (6.35-mm) WT PIPE WITH UNEQUAL STACKED CRACKS THAT MEASURE a_{ext} = 30% WT AND a_{int} = 40% WT.

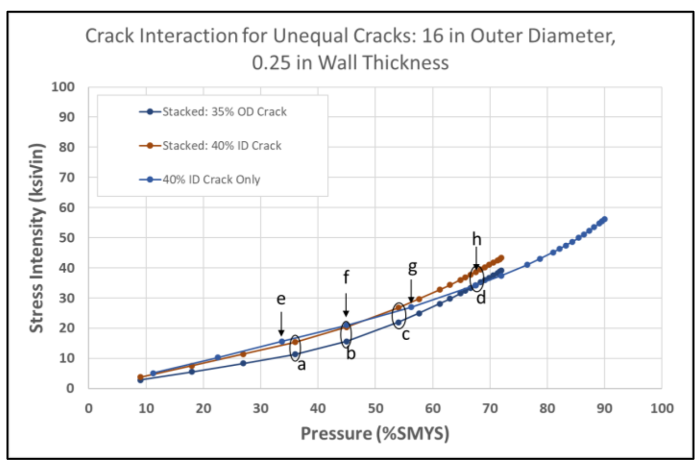

FIGURE 11: STRESS INTENSITY VERSUS PRESSURE FOR A 16-INCH (406-mm) OD AND 0.25-INCH (6.35-mm) WT PIPE

WITH UNEQUAL STACKED CRACKS THAT MEASURE a_{ext} = 35% WT AND a_{int} = 40% WT.

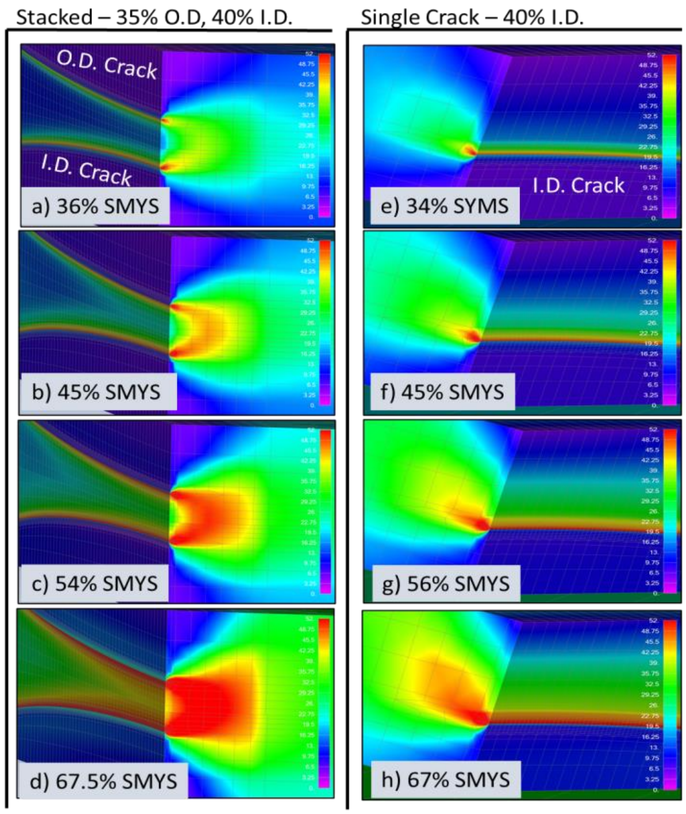

FIGURE 12: MONTAGE OF THE VON MISES STRESS FOR UNEQUAL STACKED CRACKS THAT MEASURE a_{ext} = 35% WT AND a_{int} = 40% of WT (a-d), SINGLE ID CRACK THAT MEASURES 40% WT (e-h).

3.3 Burst Pressure

Sections 3.1 and 3.2 explored how the stress intensity curves could identify crack interaction. However, the pipe material fracture toughness can predict burst pressure based upon where it intersects the stress intensity curves. Figure 13 is the same set of curves shown in Figure 3; however, two horizontal curves are introduced that represent assumed fracture toughness values for the pipe material. If fracture toughness specimens are available, the material test values can be used to determine fracture toughness. However, without toughness data, API 579 can be leveraged to provide conservative and non-conservative fracture toughness for vintage carbon steels. The conservative value of Kc = 48.3 ksi√inch (1678.4 MPa√mm) was determined based on a sulfur content >0.01% and assuming the lower 5% on exemption curve B in API 579. The less conservative value of Kc = 85.6 ksi√inch (2974.6 MPa√mm), which was derived with the sulfur content being ≤0.01% and the median value of exemption curve B in API 579. This provided a way to bound the results. A recent study [7] that tested a wide range of pre-1980's ERW pipe material could also be leveraged to assign a toughness value to predict the burst pressure for stacked cracks.

If the conservative value of Kc = 48.3 ksi√inch (1678.4 MPa√mm) is assumed for the example shown in Figure 13, the singular crack's burst pressure occurs at approximately 84% SMYS, whereas the stacked crack is shown to have a burst pressure of approximately 70% SMYS. Because the stacked cracks are shown to interact and have a large plastic zone around the ligament, it makes sense for the stacked crack to have a lower burst pressure than the single crack. The combined crack is shown to have the lowest burst pressure at approximately 60% of SMYS, which also makes sense based upon an 80% through-wall, surface-breaking crack. This exemplifies how a pipeline operator could leverage such data to better identify those cracks that require immediate mitigation versus monitoring.

Tables 4 and 5 summarize the burst pressure data for the equal and unequal stacked cracks, respectively. "N/A" indicates that, up to the simulated pressure (72% SMYS or greater), the stress intensity curve did not intersect the conservative value of Kc = 48.3 ksi√inch (1678.4 MPa√mm). Simulations would need to be run past 72% SMYS to determine their intersection; however, from an operational perspective it is unlikely for a pipeline system to be operated at higher pressures.

Note that calculated burst pressures are generally more conservative than burst pressures measured in a laboratory environment or in the field [8]. For typical vintage pipe material, this difference can be explained by burst pressure calculations being unable to account for micro-voids in material with high tramp elements [7, 9], as well as an inability to perfectly size a real-world crack found during inspection amongst other microstructural imperfections [7, 9]. Therefore, burst pressure assessments must leverage conservative fracture databases for vintage steels [7] and assume sizing inaccuracies. Thus, a stacked crack measured in a laboratory could likely produce a higher failure pressure than the numerical results indicate here. However, performing a level 3 3-D FE analysis, as was done here, can reduce the conservatism of a level 2 analysis by more accurately capturing the cracks constraint in a pipeline [7, 10].

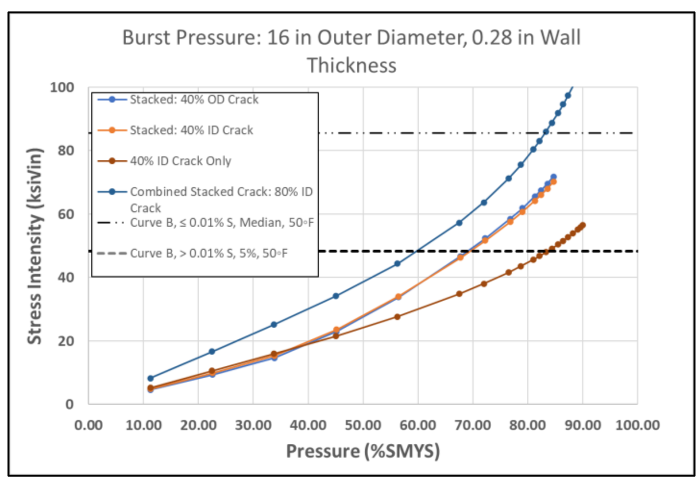

FIGURE 13: STRESS INTENSITY VERSUS PRESSURE FOR A 16-INCH (406-mm) OD AND 0.28-INCH (7.14-mm) WT PIPE

WITH EQUAL STACKED CRACKS THAT MEASURE a_{ext} = 40% WT AND a_{int} = 40% of WT. CONSERVATIVE AND MEDIAN FRACTURE TOUGHNESS CURVES ARE PROVIDED, AND THE INTERSECTION WITH THE STRESS INTENSITY CURVES REPRESENT MODELED BURST PRESSURES.

TABLE 4: CRACK MODELS DEMONSTRATE THE BURST PRESSURE FOR VARIOUS EQUAL STACKED CRACKS. st = STACKED CRACK, s = SINGLE CRACK.

Pipe OD	Pipe WT	Pipe Grade	OD and ID Crack Depths	Burst Pressure Kc = 48.3 ksi√inch	Burst Pressure Kc = 85.6 ksi√inch
Inch (mm)	Inch (mm)		%	% SMYS	% SMYS
12.75 (324)	0.219 (5.56)	X52	32.5IDst	N/A	N/A
			32.5ODst	N/A	N/A
			32.5IDs	N/A	N/A
			65IDs	65	N/A
			40IDst	70	>90
			40ODst	70	>90
			40IDs	84	N/A
			80IDs	60	80
16 (406)	0.219 (5.56)	X52	32.5IDst	N/A	N/A
			32.5ODst	N/A	N/A
			32.5IDs	N/A	N/A
			65IDs	65	N/A
			40IDst	70	>90
			40ODst	70	>90
			40IDs	84	N/A
			80IDs	58	82
16 (406)	0.25 (6.35)	X52	32.5IDst	N/A	N/A
			32.5ODst	N/A	N/A
			32.5IDs	N/A	N/A
			65IDs	65	N/A
			40IDst	70	90
			40ODst	70	90
			40IDs	84	N/A
			80IDs	60	84
16 (406)	0.281 (7.14)	X52	32.5IDst	N/A	N/A
			32.5ODst	N/A	N/A
			32.5IDs	N/A	N/A
			65IDs	65	N/A
			40IDst	70	90
			40ODst	70	90
			40IDs	84	N/A
			80IDs	60	84
16 (406)	0.314 (8.0)	X52	32.5IDst	N/A	N/A
			32.5ODst	N/A	N/A
			32.5IDs	N/A	N/A
			65IDs	65	N/A
			40IDst	70	>90
			40ODst	70	>90
			40IDs	84	N/A
			80IDs	60	84
16 (406)	0.314 (8.0)	X46	32.5IDst	N/A	N/A
			32.5ODst	N/A	N/A
			32.5IDs	N/A	N/A
			65IDs	71	N/A
			40IDst	75	>90
			40ODst	75	>90
			40IDs	87	N/A
			80IDs	65	86
24 (609)	0.281 (7.14)	X52	32.5IDst	N/A	N/A
			32.5ODst	N/A	N/A
			32.5IDs	N/A	N/A
			65IDs	65	N/A
			40IDst	70	>90
			40ODst	70	>90
			40IDs	84	N/A
			80IDs	60	85

TABLE 5: CRACK MODELS DEMONSTRATE THE BURST PRESSURE FOR VARIOUS UNEQUAL STACKED CRACKS.

Pipe OD	Pipe WT	Pipe Grade	OD/ ID Crack Depths	Burst Pressure Kc = 48.3 ksi√inch	Burst Pressure Kc = 85.6 ksi√inch
inch	inch		%	% SMYS	% SMYS
16 (406)	0.25 (6.35)	X52	30ODst	N/A	N/A
			40IDst	N/A	N/A
			35ODst	N/A	N/A
			40IDst	N/A	N/A
			40ODst	70	90
			40IDst	70	90
			20ODst	N/A	N/A
			50IDst	N/A	N/A
			22.5ODst	N/A	N/A
			50IDst	N/A	N/A
			25ODst	N/A	N/A
			50IDst	N/A	N/A
			10ODst	N/A	N/A
			60IDst	70	N/A
			40IDs	84	N/A
			50IDs	N/A	N/A
			60IDs	67	N/A
			70IDs	64	N/A
			72.5IDs	62	N/A
			75IDs	62	N/A
			80IDs	60	88
24 (609)	0.281 (7.14)	X52	30ODst	N/A	N/A
			40IDst	N/A	N/A
			35ODst	N/A	N/A
			40IDst	N/A	N/A
			40ODst	70	>90
			40IDst	70	>90

			20ODst	N/A	N/A
			50IDst	N/A	N/A
			22.5ODst	N/A	N/A
			50IDst	N/A	N/A
			25ODst	N/A	N/A
			50IDst	N/A	N/A
			10ODst	N/A	N/A
			60IDst	63	N/A
			40IDs	84	N/A
			50IDs	N/A	N/A
			60IDs	68	N/A
			70IDs	64	N/A
			72.5IDs	64	N/A
			75IDs	63	N/A
			80IDs	60	85
12.75 (324)	0.219 (5.56)	X52	30ODst	N/A	N/A
			40IDst	N/A	N/A
			35ODst	N/A	N/A
			40IDst	N/A	N/A
			40ODst	70	90
			40IDst	70	90
			20ODst	N/A	N/A
			50IDst	N/A	N/A
			22.5ODst	N/A	N/A
			50IDst	N/A	N/A
			25ODst	N/A	N/A
			50IDst	N/A	N/A
			10ODst	N/A	N/A
			60IDst	70	N/A
			40IDs	83	N/A
			50IDs	N/A	N/A
			60IDs	67	N/A
			70IDs	62	N/A
			72.5IDs	61	N/A
			75IDs	60	N/A
			80IDs	60	84
16 (406)	0.314 (8.0)	X46	30ODst	N/A	N/A
			40IDst	N/A	N/A
			35ODst	N/A	N/A
			40IDst	N/A	N/A
			40ODst	85	N/A
			40IDst	83	N/A
			20ODst	N/A	N/A
			50IDst	N/A	N/A
			22.5ODst	N/A	N/A
			50IDst	N/A	N/A
			25ODst	N/A	N/A
			50IDst	N/A	N/A
			10ODst	N/A	N/A
			60IDst	N/A	N/A
			40IDs	87	N/A
			50IDs	N/A	N/A
			60IDs	N/A	N/A
			70IDs	70	N/A
			72.5IDs	69	N/A
			75IDs	68	N/A
			80IDs	65	86

4. MODEL QUALIFICATION

A model qualification was performed by comparing burst pressure estimates produced from the FEA models of singular cracks with those produced from the CorLAS™ crack model, accounting for appropriate model error as determined by Zhang [11] and Yan [12]. Zhang et al explored the model error between predicted burst pressures using CorLAS and experimentally measured failure pressures of full-scale pipe burst tests. The model error was calculated as the ratio of experimental failure pressure to that predicted by CorLAS and follows a normal distribution with a mean of 1.02 and coefficient of variation (COV) of 13%. In a similar study, Yan et al also investigated model error, but rather than sourcing experimental burst pressure measurements, their data came from in-service and hydrotest failures, which assumed semi-elliptical crack profiles. The Yan work provided a model error with a mean of 1.27 and COV of 16%. The data in Table 4 that correspond to singular cracks were interpolated for comparison with the model error determined from Zhang and Yan. Unity lines were plotted in Figure 14 as the burst pressure's percentage of SMYS versus burst pressure (%SMYS) calculated from the CorLAS crack model. The unity curve was multiplied by $mean \times (1 \pm COV)$ for the values provided by Zhang (i.e., green dotted curve) and Yan (i.e., blue dotted curve) to represent ±1 standard deviation bounds of the CorLAS model errors. The singular internal cracks modeled in Tables 4 for the lower-bound Kc = 48.3 ksi√inch (1678.4 MPa√mm) are plotted against the unity curve and model error curves in Figure 14. The FE results from this study mainly fall within the model error bounds that were previously calculated from experimental tests and field results, lending confidence that the burst pressures and corresponding stress intensities from the FEA model are reasonable. Notable is the fact that CorLAS is most conservative compared to FEA results for cracks with 80% through-wall depth, which is consistent with Yan's findings. Figure 15 is like Figure 14, except it highlights the upper-bound Kc = 85.6 ksi√inch (2974.6 MPa√mm) data, which also demonstrate a reasonable fit to the model error.

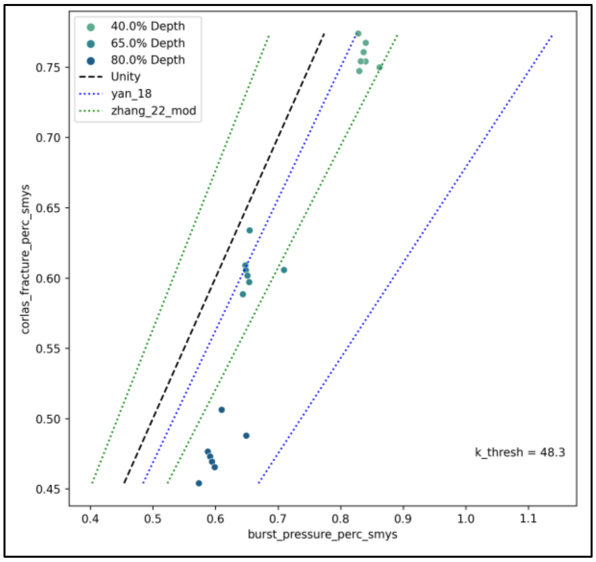

FIGURE 14: MODEL ERROR FOR SINGULAR INTERNAL CRACKS ASSUMING Kc = 48.3 ksi√inch (1678.4 MPa√mm) FROM TABLES 4 AND 5. COMPARED MODEL ERROR DETERMINED FROM LITERATURE STUDIES.

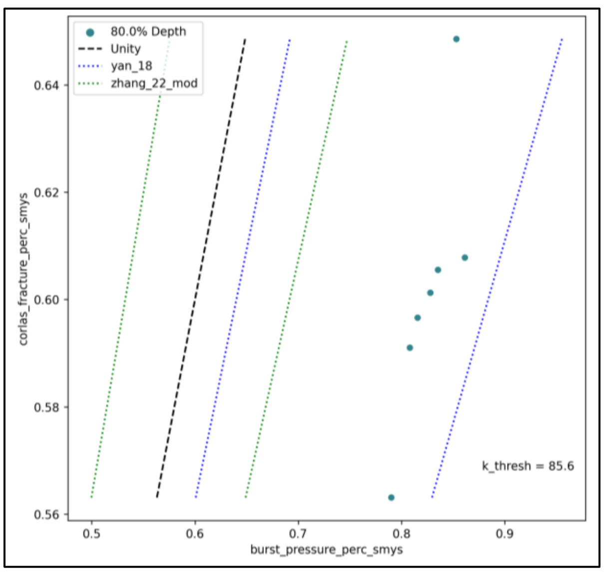

FIGURE 15: MODEL ERROR FOR SINGULAR INTERNAL CRACKS ASSUMING Kc = 85.6 ksi√inch (2974.6 MPa√mm) FROM TABLES 4 AND 5. COMPARED MODEL ERROR DETERMINED FROM LITERATURE STUDIES.

5. CONCLUSION

It has been demonstrated that 3-D elastic-plastic FEA models of multiple combinations of stacked crack sizes with various axial orientation, pipe material properties, and operating stress can improve interaction criterion from what are currently found in API 579 Part 9.

Equal sized stacked cracks exhibited no interaction up to an internal pressure of 72% of SMYS when the remaining ligament is 35% or greater, but interaction was observed when the remaining ligament is 20% or less. When observed, crack interaction was only prevalent when the pipe's internal pressure reached 45% of SMYS or greater. Unequal stacked cracks are more complex, but in general when the ligament between the external and internal crack is greater than 27% of the WT, the cracks do not interact below 72% of SMYS, assuming the internal crack is 50% of the WT or less. In excess of 50% of WT, interaction is possible at high stresses even when the ligament is greater than 27% of the WT interaction.

In addition, the burst capacity of a stacked crack can be calculated from the intersection of the material's fracture toughness along the numerically calculated stress intensity curve. From an operational perspective, it is valuable to compare the burst capacity of stacked cracks to singular cracks that are the same size as the individual stacked cracks or to a summation of the stacked crack depths. This comparison can help a pipeline operator determine the conservatism in their decision-making process.

These improved interaction criteria provide pipeline operators with an easy-to-apply methodology that reduces excess conservatism associated with legacy methods to analyze stacked cracks. In addition, this work has demonstrated the ease of modeling 3-D elastic-plastic FEA models of stacked cracks. Between the numerical model's computational speed and accuracy, the FEA models shown here could be performed following inspection to achieve high-fidelity results. Future work is required to explore stacked cracks longer than 2c = 2 inches (50.8 mm).

ACKNOWLEDGEMENTS

We thank Lyndon Lamborn, Bradley Krug, and Max Curtis of Enbridge for financial support and valuable discussions during the progression of this novel work.

REFERENCES

[1] API-579-1/ASME FFS-1 Fitness-for-Service, 2016
[2] C. Jaske and J. Beavers, "Integrity and Remaining Life of Pipe with Stress Corrosion Cracking," PRCI, 2001.
[3] J.Kiefner and K. Kolovich, "Comprehensive Study to understand Longitudinal ERW Seam Failures," PHMS, Worthington, OH, 2014
[4] G. Thorwald, M. Turnquist, and E. Jensen, "Evaluation of Interaction Behavior of Stacked Crack-Like Features," Pipeline Pigging and Integrity Management Conference, Hilton Americas-Houston, USA, Feb. 22-26, 2021.
[5] FEACrack™, Quest Integrity, 2022, URL: https://www.questintegrity.com/software-products/feacrack/
[6] Abaqus/Standard, Dassault Systemes, 2021, URL: www.abaqus.com
[7] K.E. Bagnoli, T. Neeraj, G.L. Pioszak, R.L. Holloman, G. Thorwald, C.L. Hay, "Fracture Toughness Evaluation of Pre-

1980's Electric Resistance Welded Pipeline Seam Welds," International Pipeline Conference, Calgary, Alberta, Canada, Sept 26-30, 2022.

[8] T.L. Anderson, "Realistic Burst Pressure Predictions in Pipelines with Non-Ideal Crack Profiles", Pipeline Pigging and Integrity Management Conference, Marriot Marquis Hotel, Houston, USA, Feb. 18-22, 2019.

[9] P. Sarosi, F. Furmanski, W.C. Eiise, Carpenter. D.L., M.G. Myers, N.M. Callen, and T. Neeraj, "Damage Evolution During Fracture by Correlative Microscopy with Hyperspectral Electron Microscopy and Laboratory-Based Microtomography," *Sci. Adv.*, vol. 8, 2022.

[10] F. Furmanski and T. Neeraj, "Pin-loaded SENT specimen for constraint-matched fracture testing of radially propagating longitudinal cracks in thin-walled pipelines," Engineering Fracture Mechanics, vol. 268, June 2022.

[11] X. Zhang, Q. Zheng, J. Leung, S. Adeeb, "Reliability-Based Assessment of Cracked Pipelines Using Monte Carlo Simulation Technique with CorLAS™" Pressure Vessels and Piping Conference, Las Vegas, Nevada, July 17-22, 2022.

[12] J. Yan, S. Zhang, S. Kariyawasam, M. Pino, T. Liu, "Validate Crack Assessment Models with In-Service and Hydrotest Failures," International Pipeline Conference, Calgary, Alberta, Canada, Sept 24-28, 2018.

